ELSEVIER

Journal of Molecular Catalysis A: Chemical 136 (1998) 75–84

JOURNAL OF MOLECULAR CATALYSIS A: CHEMICAL

Electrocatalytic oxidation of preadsorbed monolayer of CO on polycrystalline Pt_{60}–Ru_{40} electrocatalyst: nucleation and growth of oxygen-containing species

M. Metikoš-Huković *, S. Omanović

Department of Electrochemistry, Faculty of Chemical Engineering and Technology, University of Zagreb, Savska 16, POB 177, 10000 Zagreb, Croatia

Received 24 November 1997; accepted 18 December 1997

Abstract

The kinetics and mechanism of nucleation and growth of oxygen-containing-species, during the electro-oxidation of preadsorbed saturated monolayer of CO on polycrystalline Pt_{60}–Ru_{40} electrodeposited catalysts, were investigated in a CO-free perchloric acidic solution, using stripping voltammetry and potentiostatic pulse technique. The surface composition of investigated catalysts was determined using XPS. The plots of CO oxidation rate vs. time (j–t curves) displayed responses quite typical for the processes controlled by the nucleation and growth phenomena. Therefore, the overall rate of the CO oxidation reaction can be expressed in terms of the rate of nucleation and growth of oxygen-containing species in adsorbed CO monolayer. With the increase in CO oxidation potential above +0.5 V vs. NHE, the change from a 2D-kinetically controlled nucleation to a 3D-diffusionally controlled nucleation mechanism was observed. Enhanced electrocatalytic activity of the investigated Pt–Ru surface toward CO electro-oxidation, compared to pure Pt surface, was discussed in terms of the propensity of Ru atoms nucleation sites toward the adsorption of oxygen-containing species and in respect to the observed difference in the intrinsic rate constants for CO oxidation on Pt vs. Ru surface atoms. Potentiostatic and voltammetric CO stripping experiments clearly showed the bifunctional character of our Pt–Ru catalyst, with enhanced synergistic properties.

Keywords: Carbon monoxide; Platinum; Ruthenium; Nucleation; Electrocatalysis; Synergism; Bifunctional mechanism

1. Introduction

During the past few decades a number of investigations have been performed in an attempt to find suitable anodes that act as electrocatalysts for fuel-cells. The results have shown that platinum is one of the catalysts of choice in acid medium. On the other hand, ‘poisoning’ of its surface even with the trace levels of irreversibly adsorbed carbon monoxide [1], which appears as an intermediate reaction product or an impurity, depending on a type of a fuel-cell used, leads to a drastically decreased fuel-cell power density [2]. Therefore, the adsorption and oxidation of carbon monoxide have been the subjects of many studies [3–16]. Various electrochemical and spectroscopic methods, experi-

* Corresponding author. e-mail: mmetik@marie.fkit.hr

1381-1169/98/$ - see front matter
PII: S1381-1169(98)00014-4

mental conditions, single crystal and polycrystalline electrodes with different surface preparation or surface states have been employed [3–27]. It was found that adsorption of carbon monoxide depends strongly on the Pt-electrode structure, giving rise to the observed structural effects during electrocatalytic oxidation of small organic molecules [28,29].

However, CO molecules, irreversibly adsorbed on Pt electrode, can be oxidatively removed from a Pt surface by electro-oxidation to CO_2, for what the oxygen-containing species or activated water molecules have to be present at the surface. The adsorption of oxygen-containing species on platinum in acidic electrolytes occurs at high anodic potentials; consequently, a poison removal by electro-oxidation can occur only at potentials substantially anodic to the reversible potential of hydrogen or methanol oxidation. Due to that high anodic overpotential for fuel-cell operation, considerable effort has been devoted in ascertaining ways to facilitate the adsorption of oxygen-containing species at lower anodic potentials. The problem has been partially solved by modification of the Pt surface with the addition of the second metal (ad-metal), thus producing the so-called bimetallic electrocatalysts: Pt–Sn [30,31], Pt–Rh [32], Pt–Ru [10–13], Pt–Bi [30,33–39], Pt–Cu [35,40].

Nevertheless, a number of studies showed that the platinum surface modified by ruthenium is the most active catalyst for oxidation of small organic molecules [10–13,41–43]. The promoting effect of this metal is attributed to the bifunctional mechanism, which was proposed by Watanabe and Motoo [41]. Despite a large number of studies performed on variously produced Pt–Ru electrodes, only Gasteiger et al. [10,13,42,43] have optimised the catalytic Pt–Ru system for CO electro-oxidation, with UHV-prepared and thus well-characterised Pt–Ru alloys. The reaction mechanism (major reaction pathway) of the electrooxidation of preadsorbed saturated CO monolayer on Pt and Ru single crystal electrodes and on well-characterised Pt–Ru alloy electrodes in CO-free acid solution was well formulated in their papers [10, 13,42,43]. Below, we will briefly outline their development in order to elucidate the possible reasons for the strong synergism displayed by Pt–Ru electrodes.

It is believed that the electro-oxidation of CO_{ads} on an electrode surface in an electrolyte solution (i.e., under electrochemical conditions) occurs analogously to the oxidative removal of CO_{ads} on a Pt surface in the gas phase, which proceeds via Langmuir–Hinshelwood mechanism, i.e., by reaction of chemisorbed CO with chemisorbed oxygen [10,13,42–45]. However, the source of oxygen in those two media is very different, i.e., O_2 vs. H_2O. The oxygen containing species in the electrochemical environment are most likely in the form of adsorbed hydroxyl species, OH_{ads}, whereas the adsorbed state of oxygen in UHV is O_{ads}. Nevertheless, a striking similarity exists between the properties inferred from the gas-phase data and observed equally strong adsorption of CO on both Pt and Ru electrodes in acid electrolytes.

The role of Ru atoms on Pt–Ru surface has been attributed to the fact that the adsorption of oxygen-containing species occurs at significantly more negative potentials on its sites in comparison to Pt [46,47]. This is in correspondence with higher activity of Ru towards oxygen, highlighting the importance of bare Ru sites to initiate the nucleation of OH_{ads} on Pt–Ru surface, thereby supporting the concept of the bifunctional character of the CO electro-oxidation process on these catalysts. Hence, Ru sites act as OH_{ads} species collectors, which then catalyse the oxidation of CO molecules preferentially bonded on the neighbouring Pt atoms. Therefore, the most pronounced synergistic effect of the Pt–Ru catalysts toward CO electrooxidation was obtained with the optimum surface composition of Pt:Ru = 50:50, thus balancing between the maximum of surface sites to 'seed' the electrode with OH_{ads} at low potentials and maximising the number of Pt/Ru pair sites, with reduced adsorption strength of OH_{ads}, as compared to Ru/Ru pair sites [10,13,48].

Due to the huge significance of oxygen-containing species in the overall mechanism of oxidation of small organic molecules, we performed in-situ potentiostatic measurements in order to investigate the kinetics of nucleation and growth of the oxygen-containing species formed in a CO monolayer irreversibly adsorbed on Pt–Ru electrocatalyst. There are only few papers, based on the potential-step measurements on Pt–Ru [10] and Pt [10,24,49–55], which deal with this subject, but to our best knowledge, this is the first time that the electrodeposited Pt–Ru electrocatalyst is studied in order to investigate the kinetics and mechanism of nucleation and growth of oxygen-containing species on its surface, which actually controls the rate of CO oxidation if the surface is initially covered by a monolayer of CO and subsequently exposed to the conditions at which oxidation reaction occurs. It is shown that the potentiostatic technique is a precious tool in this type of investigations. The results have been discussed on the basis of theoretical mathematical models, developed primarily for the electrodeposition of metals on a conductive substrate, which were highly applicable in our case, too.

2. Experimental

Polycrystalline Pt–Ru electrocatalysts were made by the electrodeposition of electroactive components on an Au substrate at a constant potential, $E_{ad} = 0$ V vs. NHE during 15 min, using the solutions of H_2PtCl_6 and $RuCl_3$ in 1 M $HClO_4$, with Pt and Ru in stoichiometric ratio 1:1. The real surface composition of this electrode was determined using X-ray photoemission spectroscopy (XPS), which revealed the stoichiometric ratio of Pt:Ru = 60:40.

A standard three-electrode cell was used in all experiments. The counter electrode was a platinum electrode and the reference electrode was a standard calomel electrode. However, potentials in this paper are referred to the normal hydrogen electrode (NHE). All measurements were performed at 21 ± 2°C in O_2 free 1 M $HClO_4$ electrolyte.

Stripping voltammetry curves and the current-time transients resulting from the potentiostatic experiments were recorded digitally. The equipment was comprised of an EG&G PAR Model 273 potentiostat/galvanostat controlled by a PC. In XPS measurements, the X-ray excitation source was a Mg anode (MgKa line). In all cases, the outgoing electrons were analysed using a Vacuum Science Workshop (VSW) 180°-hemispherical analyser in the FAT 50 mode. Data acquisition and manipulation was performed by the VSW E-C 7.02 program package.

In order to avoid mass-transfer resistance, all experiments were performed with an adsorbed monolayer of CO. Carbon monoxide adsorption was carried out from the CO saturated solution at an adsorption potential of $E_{ad} = +0.1$ V during 2 min. The excess of CO dissolved in the solution was then removed by stirring the N_2 during the following 15 min, maintaining the electrode at the adsorption potential. Therefore, the only CO present in the system during the measurements was that adsorbed on the electrode surface.

Stripping voltammetry measurements were performed with the initially adsorbed CO monolayer, starting the scan from the adsorption potential down to the cathodic potential limit (+0.05 V vs. NHE), then up to the anodic potential limit (depending on the electrode material) and finally back to the adsorption potential. Anodic potential limit for the Pt–Ru electrode was below +0.9 V due to the onset of Ru dissolution. In each experiment, two successive cycles were made: the first was due to CO oxidation and the second due to the characterisation of the pure electrode surface.

Potentiostatic measurements were performed according to the following procedure: the electrode surface was initially covered by a monolayer of CO as described previously. Next, the potential step was applied from the adsorption

potential to a potential domain of CO oxidation. The rate of oxidation was monitored by recording the resulting current transients. In order to assess the completeness of the CO oxidation, a stripping voltammogram was recorded. After several cycles between the standard potential limits, the above potentiostatic experiment was repeated in the absence of adsorbed CO to record the currents resulting from the pseudocapacitance of the electrodes.

3. Results and discussion

3.1. Stripping voltammetry measurements

Although the oxidation of carbon monoxide under the potentiodynamic conditions has been a subject of a number of investigations [10–15,23,56], we will briefly summarise the stripping voltammetry results obtained on a Pt–Ru electrocatalyst prepared in our laboratory. These results are basically comparable to those performed in a similar way and presented in the literature [10–13,23]. In this work they are used as a basis for choosing the potential regions for a potential step experiment and discussion of the results.

Prior to further discussion, it has to be said that in all experiments presented in this paper the catalyst surface was covered with an essentially saturated monolayer of CO, which was obvious from the complete blocking of the pseudocapacitive currents in the hydrogen potential region (Fig. 1a and b).

Fig. 1a shows the stripping voltammogram for the oxidation of CO on Pt–Ru electrocatalyst (solid line), together with the voltammogram recorded on pure catalyst after CO removal (dashed line). As can be seen, anodic stripping scan (solid line) is characterised by a sharp oxidation peak at the potential of $+0.45$ V, which corresponds to oxidation of CO molecules irreversibly adsorbed on the catalyst's surface [10,13]. The same figure shows the stripping voltammetry results obtained with pure

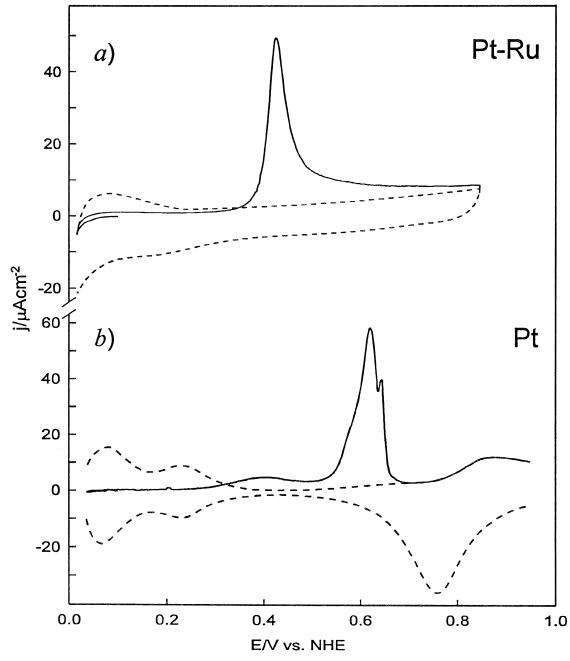

Fig. 1. Stripping voltammograms for (a) Pt–Ru and (b) Pt electrodes recorded in 1 M $HClO_4$ solution in the presence of a CO monolayer irreversibly adsorbed on the electrode surface at potential $E_{ads} = +0.1$ V (solid line), and in a CO-free solution (dashed line). Sweep rate ν was 10 mV s^{-1}.

Pt electrocatalyst under the identical experimental conditions (Fig. 1b). In comparison to Pt–Ru, CO oxidation peak on Pt is located at somewhat positive potentials, around $+0.62$ V. The observed potential difference of the CO oxidation peaks ($\Delta E = 0.17$ V) is a clear evidence of enhanced electrocatalytic activity of the Pt–Ru electrocatalyst in comparison to pure Pt, which is obviously influenced by the presence of Ru atoms at the surface. In addition, comparing the potential values for the CO oxidation peaks obtained at investigated Pt and Pt–Ru surfaces to those at pure Ru [10,12,15], which actually lays between them, it is obvious that Pt–Ru electrocatalyst displays strikingly synergistic properties, which could not be rationalised by a simple linear superposition of the properties of pure metals [10].

Although the Pt–Ru electrode showed enhanced catalytic behaviour, which was manifested through the shift of the oxidation peak

potential to more negative value in comparison with pure metal components, it is worth noting that the oxidation current after the sharp oxidation peak slowly decreases in the broad potential range (Fig. 1a), and the complete oxidation of CO monolayer is not achieved below the anodic potential limit (+0.85 V). However, this is not the case with the Pt electrode, where the CO oxidation is completed below +0.7 V (Fig. 1b), and the currents in the first and second scans become equal at this potential.

3.2. Potentiostatic measurements

Potentiostatic measurements were performed in the potential range between +0.4 and +0.7 V, where electro-oxidation of CO to CO_2 takes place, in order to investigate the kinetics and mechanism of nucleation and the growth of the oxygen-containing species, OH, formed in a CO monolayer irreversibly adsorbed on a Pt–Ru surface.

A series of representative current-time transients obtained for a Pt–Ru electrocatalyst, after correction against the pseudocapacitance current, are presented in Fig. 2. An example of a correction procedure is showed in the Fig. 3, where the transients recorded on the electrode surface covered with the CO monolayer (dashed line), after CO stripping, i.e., pseudocapacitance transient (dotted line), and the resulting transient after correction due to the pseudocapacitance current are presented. Due to the big differences in the oxidation times at each potential, transients from Fig. 2 are shown against the logarithm of time, for ease of comparison.

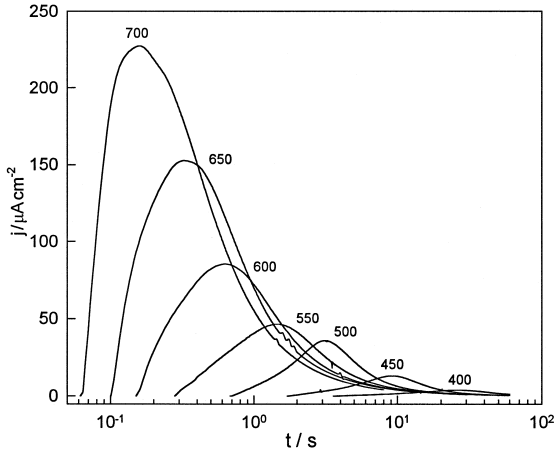

Fig. 2. Potentiostatic transients for the nucleation and growth of oxygen-containing species on the Pt–Ru electrode covered with a CO monolayer in 1 M $HClO_4$ solution, after correction due to the pseudocapacitive current. Potentials are expressed in mV. The potential step was applied from the CO adsorption potential, $E_{ads} = +0.1$ V, to the various oxidation potentials showed in the figure.

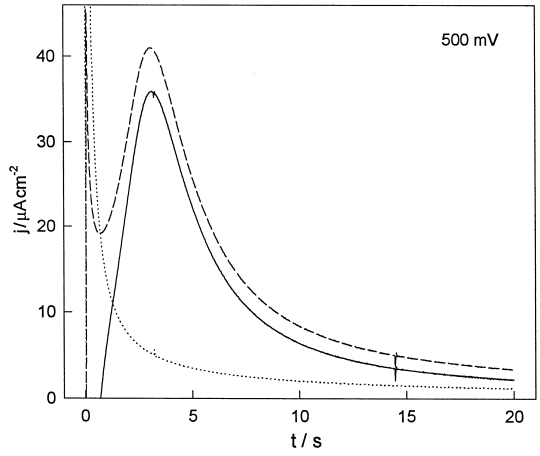

Fig. 3. An example of a row potentiostatic transient recorded on a CO covered Pt–Ru surface (dashed line), after CO stripping (dotted line—pseudocapacitive current) and resulting corrected transient (solid line).

The behaviour of transients (Fig. 2) is quit typical for the process of nucleation and growth under the anodic bias, i.e., the presented transients showed the marked maximums, which are characterised by the increase of a current density j_m and decrease of a time of maximum t_m, as the applied oxidation potential is made more positive.

However, to determine the type of the nucleation and growth mechanism of the oxygen-containing species on a Pt–Ru surface, transients recorded at various potentials were normalised to the coordinates of their maximums j_m and t_m and compared with the theory through Eqs. (1) and (2) [50,57–61]:

$$\frac{j}{j_m} = \frac{t}{t_m}\exp\left(\frac{t_m^2 - t^2}{2t_m^2}\right) \quad (1)$$

$$\frac{j}{j_m} = \sqrt{\frac{1.9542}{t/t_m}} \left\{ 1 - \exp\left(-1.2564 \frac{t}{t_m} \right) \right\} \quad (2)$$

A set of such normalised transients is shown in Fig. 4. The solid line represents the kinetically controlled two-dimensional (2D) instantaneous nucleation and growth response, described by Eq. (1), and the dashed line corresponds to the diffusionally controlled three-dimensional (3D) instantaneous nucleation and growth response, described by Eq. (2).

It is obvious that the experimental transients fit neither of these theoretical responses in the entire time region, but lay between them. At lower potential values (below +0.5 V), the nucleation of oxygen-containing species on the Pt–Ru surface (see the increasing portion of the curves at short times) could be described by 2D instantaneous and progressive type of mechanism, i.e., the data lay between these two theoretical responses (solid and dotted lines, respectively). In this potential region, the nucleation and growth of 'oxygen' islands is uniquely defined by the 2D mechanism at shorter growth time. With the increase of potential above +0.5 V, the influence of a diffusion process (the appearance of the tailing of the transients at longer time) and 3D nuclei growth becomes significant. Therefore, the nucleation and growth of the oxygen-containing species on Pt–Ru surface could be, in this upper potential region, defined by mixed 2D and 3D nucleation and growth mechanisms. The appearance of the diffusion process is, probably, related to the surface diffusion of oxygen-containing species from its nucleation sites to the reaction sites where the oxidation of CO proceeds.

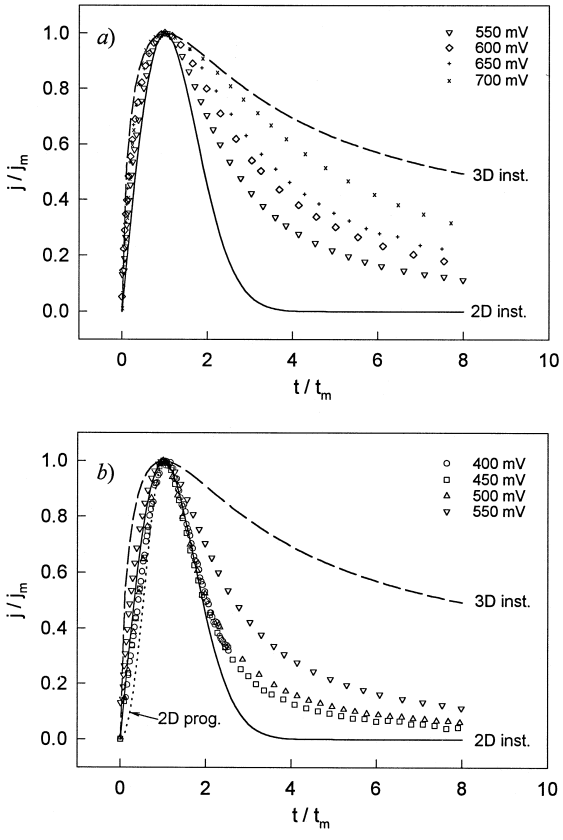

Fig. 4. Transients from Fig. 2 normalised to the coordinates of their maximums (symbols), plotted along with the theoretical 2D and 3D nucleation and growth responses (lines) for the Pt–Ru electrode covered with the CO monolayer in 1 M $HClO_4$.

According to the bifunctional mechanism [10,41], the electro-oxidation of CO molecules adsorbed onto the Pt–Ru surface could be presented in two major steps: (i) nucleation and growth of oxygen-containing species on the Ru sites:

$$Ru + H_2O \overset{E_{Ru}}{\leftrightarrow} OH_{ads} + H^+ + e^- \quad (3)$$

which then can initiate (catalyse) the further electro-oxidation of CO molecules adsorbed on either Pt or Ru neighbouring sites, i.e., (ii) bimolecular reaction between nucleated oxygen-containing species OH_{ads}, and adsorbed carbon monoxide:

$$CO_{ads} + OH_{ads} \overset{rds}{\rightarrow} CO_2 + H^+ + e^- \quad (4)$$

Our results can be explained qualitatively in terms of surface reactions (3) and (4) with the assumption that the reaction (4) is the rate-determining step in the overall mechanism of CO oxidation on Pt–Ru and reaction (3) is in quasi-equilibrium.

On the basis of Eq. (4), assuming simple Langmuir–Hinshelwood kinetics, CO oxidation rate on Pt–Ru surface may be formulated as:

$$r_{(x)} = k_{(x)}\theta_{CO}\theta_{OH} \quad (5)$$

where $k_{(x)}$ represents the substrate dependent rate constant, and θ_{CO} and θ_{OH} represent the surface coverage of the catalyst with adsorbed CO and oxygen-containing species OH_{ads}, respectively. Transients recorded on the Pt–Ru electrode at potentials below +0.5 V showed that the rates of reactions (3) and (4) are comparable, which is quite obvious from the obtained 2D responses. However, with an increase in potential above +0.5 V, the rate of the formation of OH_{ads} species becomes much larger, and the reaction (4) is not any more capable to 'consume' all the OH_{ads} formed, which results in 3D nuclei growth. This becomes more apparent with increase of oxidation potential (see Fig. 4).

In order to elucidate the nucleation and growth rates of the oxygen-containing species at applied oxidation potential, potentiostatic transients from Fig. 2 were further treated. The inverse of time, corresponding to the current maximum, $1/t_m$, as well as the current density of a maximum, j_m, can be taken as a measure of the reaction rate [24,50,58,59]. Fig. 5 shows the plots of the logarithm of t_m and j_m against the applied potential.

The rough inspection of the dependencies presented in Fig. 5 generally showed that with the increase of the electrode potential, the reaction rate also increases in entire potential region (i.e., j_m increases and t_m decreases, see Fig. 5). This points to the conclusion that the concentration (coverage) of the adsorbed OH_{ads} species at the perimeter line of the formed islands of oxygen-containing species varies (increases) with the oxidation potential.

However, the close inspection of the results presented in Fig. 5 showed that the entire potential region can be divided into two potential sub-regions, with the breaking point around

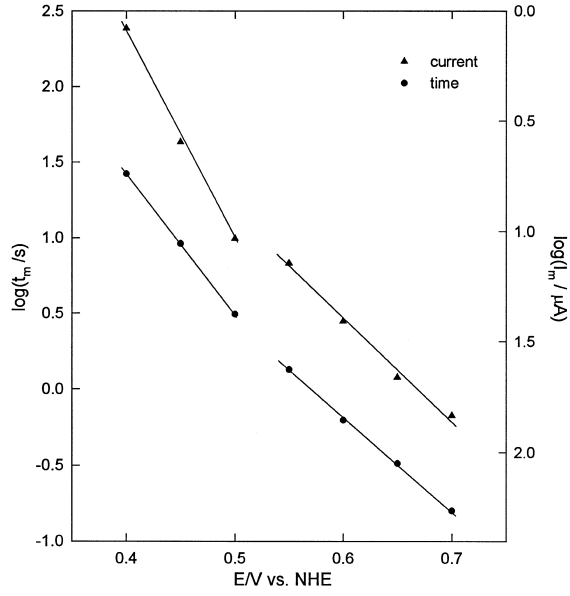

Fig. 5. Dependencies of log t_m and log j_m corresponding to the maximum of the transients from Fig. 2, plotted against the applied potential, for the Pt–Ru electrode covered with a CO monolayer in 1 M $HClO_4$.

+0.5 V. The same is obtained if we expand the increasing portion of the transients from Fig. 3 (short time). All the data recorded at potentials below +0.5 V have identical j against t dependence, different from that recorded at potentials above +0.5 V.

From combined voltammetric and XPS [47] as well as elipsometric experiments [46] it was concluded that the formation of OH_{ads} on bulk Ru commences at electrode potential of about +0.2 V, which is significantly negative than the onset of OH_{ads} formation on Pt, such that the nucleation of OH_{ads} on bare Ru surface atoms (i.e., without adsorbed CO) was assumed to be in quasi-equilibrium according to the reaction (3). Finally, the basic hypothesis of Ru-induced nucleation of OH_{ads} around +0.2 V was additionally supported from the decreasing activity of pure Ru toward H_2 oxidation above this potential value. These experimental findings were supported by atom superposition and electron delocalization calculations, showing that the activation energy for the nucleation of OH_{ads} from water, Eq. (3), is significantly reduced by

the presence of Ru in Pt–Ru, if compared to pure Pt [48].

Therefore, the lower potential sub-region (Fig. 5) could be ascribed solely to the Ru influence on the oxygen-containing species formation, and in this potential domain oxidation of CO is fully in accordance with the bifunctional mechanism. The bimolecular reaction rate constant $k_{(x)}$ in Eq. (5) is, therefore, related solely to the Ru/Pt pair sites, leading to the pronounced synergism of the Pt–Ru surface, in contrast to the slow kinetics observed for a pure Ru surface [10,13].

Looking back to the Fig. 1, it is worth noting that the commencing of the CO oxidation peak tail-end on the Pt–Ru electrocatalyst coincides well with the onset potential for CO oxidation on the pure Pt (ca. $+0.5$ V). Further, the change in the nucleation and growth mechanism was noted above $+0.5$ V (Fig. 4), as well as, the change in the dependence of the reaction rate on the applied potential (Fig. 5). This points to the conclusion that above $+0.5$ V, the oxygen-containing species adsorption occurs on the Pt sites, too, and the overall nucleation and growth mechanism is in this potential domain very complex and dependent on both Ru and Pt; above $+0.5$ V the nucleation of OH_{ads} on bare Pt surface atom (i.e., free of adsorbed CO) was assumed to be in quasi-equilibrium:

$$Pt + H_2O \overset{E_{Pt}}{\leftrightarrow} OH_{ads} + H^+ + e^- \quad (6)$$

Hence, bimolecular reaction rate constant from Eq. (5) cannot be considered anymore to be related only to the Ru/Pt pair sites, but to both Ru/Pt and Pt/Pt sites. The change in slope of the dependencies from Fig. 5 could be indirectly related to the change of the reaction rate constant $k_{(x)}$, and therefore, the lower value of the slope (consequently, lower $k_{(x)}$) points to the decreased synergetic effect of Pt–Ru surface in this upper potential region, although the reaction rate generally increases with increase of oxidation potential. Thus, the bimolecular reaction rate constant $k_{(x)}$ seems to be not only substrate-dependent, but potentially dependent, too. Further, it could be said that the bifunctional mechanism, according to which Ru sites acts as OH_{ads} species collectors and Pt sites as reaction sites (the best Pt:Ru ratio is therefore 1:1), is not in full meaning valid in this potential region, due to the adsorption of OH_{ads} species onto the Pt sites, too.

4. Conclusions

The kinetics and mechanism of nucleation and growth of oxygen-containing species, during the electro-oxidation of preadsorbed saturated monolayer of CO on polycrystalline Pt_{60}–Ru_{40} electrodeposited electrodes (catalysts), were investigated in a CO-free perchloric acidic solution, using stripping voltammetry and potentiostatic pulse technique.

The stripping voltammetry results were in accordance with those presented in the literature, and showed an enhanced electrocatalytic activity of the Pt–Ru catalyst toward CO oxidation, in comparison to the Pt catalyst, which was indicated by a shift of the CO oxidation potential to more negative values.

The kinetics and mechanism of nucleation and growth of the oxygen-containing species, formed inside the CO monolayer adsorbed on Pt–Ru surface, was investigated using potentiostatic pulse technique. The plots of CO oxidation rate vs. time (j–t curves) displayed responses quite typical for the processes controlled by the nucleation and growth phenomena. Therefore, the overall rate of the CO oxidation reaction was expressed in terms of the rate of nucleation and growth of oxygen-containing species in adsorbed CO monolayer.

It was shown that two different reaction mechanisms of oxygen-containing species nucleation and growth exist in the investigated potential region, with the breakpoint potential around $+0.5$ V. The first, lower potential region was ascribed solely to the influence of Ru atoms on the nucleation of oxygen-containing

species. However, in the second potential region (above +0.5 V) Pt sites become active toward OH_{ads} adsorption, too, and nucleation of oxygen-containing species takes place simultaneously on both Pt and Ru sites.

The nucleation and growth of oxygen-containing species on Ru atoms followed a 2D type of kinetically controlled mechanisms, whereas in the potential region of both Pt and Ru influence, a 3D type of nucleation and growth mechanism, with diffusion control, prevailed. An increase of CO oxidation potential above +0.5 V was followed with both increasing influence of the 3D mechanism and diffusion control. However, the lower potential region, with the Ru influence on the formation of OH_{ads} species, is of importance for fuel-cells operation, where the strong synergism of Pt–Ru surface is present, as well as, bifunctional mechanism in its full meaning.

A strong enhancement in the catalytic activity of Pt–Ru electrode, compared to pure Pt, was attributed to the property of Ru atoms to nucleate oxygen-containing species at low potentials, thereby supporting the concept of the bifunctional character of investigated Pt–Ru surfaces. Stripping voltammetry experiments showed strong synergistic effect of Pt–Ru surface, too, with the catalytic shift of the CO stripping peak to more negative potentials compared to pure Pt. Synergism of this electrode was attributed to a uniquely active state of OH_{ads} on Pt/Ru pair sites.

References

[1] H.P. Dhar, L.G. Christner, A.K. Kush, J. Electrochem. Soc. 134 (1987) 3021.
[2] R.A. Lemons, J. Power Sources 29 (1990) 251.
[3] S.R. Bare, P. Hofmann, D.A. King, Surf. Sci. 144 (1984) 347.
[4] K. Kunimatsu, W.G. Golden, H. Seki, M.R. Philpott, Langmuir 1 (1985) 245.
[5] K. Kunimatsu, H. Saki, W.G. Golden, J.G. Gordon II, M.R. Philpott, Langmuir 2 (1986) 464.
[6] Y. Ikezawa, H. Saito, H. Fujisawa, S. Tsuji, G. Toda, J. Electroanal. Chem. 240 (1988) 281.
[7] Y. Ikezawa, H. Fujisawa, F. Ishii, Surf. Sci. 218 (1989) 246.
[8] C. Lamy, J.M. Leger, J. Clavilier, R. Parsons, J. Electroanal. Chem. 150 (1983) 71.
[9] J. Sobkowski, A. Czerwinski, J. Phys. Chem. 89 (1985) 365.
[10] H.A. Gasteiger, M. Markovic, P.N. Ross Jr., E.J. Cairns, J. Phys. Chem. 98 (1994) 617.
[11] M. Krausa, W. Vielstich, J. Electroanal. Chem. 379 (1994) 307.
[12] R. Ianniello, V.M. Schmidt, U. Stimming, J. Stumper, A. Wallau, Electrochim. Acta 39 (1994) 1863.
[13] H.A. Gasteiger, N.M. Markovic, P.N. Ross Jr., J. Phys. Chem. 99 (1995) 8290.
[14] J. Clavilier, J.M. Orts, R. Gómez, J.M. Feliu, A. Aldaz, J. Electroanal. Chem. 404 (1996) 281.
[15] T. Frelink, W. Visscher, A.P. Cox, J.A.R. van Veen, Ber. Bunsenges. Phys. Chem. 100 (1996) 599.
[16] K.A. Friedrich, K.-P. Geyzers, U. Linke, U. Stimming, J. Stumper, J. Electroanal. Chem. 402 (1996) 123.
[17] J.M. Leger, B. Beden, C. Lamy, S. Bilmes, J. Electroanal. Chem. 170 (1984) 305.
[18] J.M. Feliu, A. Fernandez-Vega, A. Aldaz, J. Clavilier, J. Electroanal. Chem. 256 (1985) 149.
[19] F. Kitamura, M. Takahashi, M. Ito, J. Phys. Chem. 92 (1988) 3320.
[20] Y. Kinomoto, S. Watanabe, M. Takahashi, M. Ito, Surf. Sci. 242 (1991) 538.
[21] I. Oda, M. Ito, Chem. Phys. Lett. 203 (1993) 99.
[22] J.M. Pérez, E. Muñoz, E. Morallón, F. Cases, J.L. Vázquez, A. Aldaz, J. Electroanal. Chem. 368 (1994) 285.
[23] O. Wolter, J. Heitbaum, Ber. Bunsenges. Phys. Chem. 88 (1984) 6.
[24] B. Love, J. Lipkowski, in: M.P. Soriaga (Ed.), Electrochemical Surface Science: Molecular Phenomena at Electrode Surfaces, Chap. 33., A.C.S. Symposium Series No. 378, Washington DC, 1988.
[25] B. Beden, C. Lamy, N.R. De Tacconi, A.J. Arvia, Electrochim. Acta 35 (1990) 691.
[26] A.M. De Becdeliévre, J.J. De Becdeliévre, J. Clavilier, J. Electroanal. Chem. 294 (1990) 97.
[27] S.G. Sun, J. Clavilier, J. Electroanal. Chem. 236 (1987) 95.
[28] B. Beden, S. Juanto, J.M. Leger, C. Lamy, J. Electroanal. Chem. 238 (1987) 323.
[29] C. Lamy, J.M. Leger, J. Chim. Phys. 88 (1991) 1649, and references therein.
[30] S.A. Campbell, R. Parsons, J. Chem. Soc., Faraday Trans. 88 (1992) 833.
[31] A.B. Anderson, E. Grantscharova, P. Shiller, J. Electrochem. Soc. 142 (1995) 1880.
[32] P.N. Ross, K. Kinoshita, A.J. Scarpellio, P. Stonehart, J. Electroanal. Chem. 59 (1975) 177.
[33] J. Clavilier, J.M. Feliu, A. Aldaz, J. Electroanal. Chem. 243 (1988) 419.
[34] M. Osawa, H. Sakurai, K. Ito, W. Suëtaka, Chem. Lett., (1990) 839.
[35] S.C. Chang, M.J. Weaver, Surf. Sci. 241 (1991) 11.
[36] R.W. Evans, G.A. Attard, J. Electroanal. Chem. 345 (1993) 337.
[37] W.F. Lin, S.G. Suna, Z.W. Tian, J. Electroanal. Chem. 364 (1994) 1.
[38] E. Herrero, J.M. Feliu, A. Aldaz, J. Electroanal. Chem. 36 (1994) 101.

[39] E. Herrero, J.M. Feliu, A. Aldaz, J. Catalysis 152 (1995) 264.
[40] B. Bittins-Cattaneo, E. Santos, W. Vielstich, Electrochim. Acta 31 (1986) 1495.
[41] M. Watanabe, S. Motoo, J. Electroanal. Chem. 60 (1975) 267.
[42] H.A. Gasteiger, N. Markoviæ, P.N. Ross Jr., E.J. Cairns, J. Phys. Chem. 97 (1993) 12020.
[43] H.A. Gasteiger, N. Markoviæ, P.N. Ross Jr., E.J. Cairns, J. Electrochem. Soc. 141 (1994) 1795.
[44] C.T. Campbell, G. Erte, H. Knipers, I. Segner, J. Chem. Phys. 73 (1980) 5862.
[45] C.H.F. Peden, D.W. Goodman, M.D. Weisel, F.M. Hoffmann, Surf. Sci. 253 (1991) 44.
[46] E. Ticanelli, J.G. Beery, M.T. Paffett, S. Gottesfeld, J. Electroanal. Chem. 258 (1989) 61.
[47] M. Vukovic, T. Valla, M. Milun, J. Electroanal. Chem. 356 (1993) 81.
[48] A.B. Anderson, E. Grantscharova, J. Phys. Chem. 99 (1995) 9143.
[49] E. Santos, E.P.M. Leiva, W. Vielstich, Electrochim. Acta 36 (1991) 555.
[50] C. McCallum, D. Pletcher, J. Electroanal. Chem. 70 (1976) 277.
[51] S.A. Bilmes, A.J. Arvia, J. Electroanal. Chem. 361 (1993) 159.
[52] S. Gilman, J. Phys. Chem. 66 (1962) 2657.
[53] S. Gilman, J. Phys. Chem. 67 (1963) 78.
[54] S. Gilman, J. Phys. Chem. 67 (1963) 1898.
[55] S. Gilman, J. Phys. Chem. 68 (1994) 70.
[56] J.M. Feliu, J.M. Orts, R. Gómez, A. Aldaz, J. Electroanal. Chem. 372 (1994) 265.
[57] Southampton Electrochemistry Group, in: Instrumental Methods in Electrochemistry, Chap. 9, Ellis Horwood, Chichester, 1985.
[58] M. Fleischman, H.R. Thirsk, in: P. Delahay (Ed.), Advances in Electrochemistry and Electrochemical Engineering: Metal Deposition and Electrocrystallization, Vol. 3, Interscience, New York, 1963.
[59] B. Scharifker, G. Hills, Electrochim. Acta 28 (1983) 879.
[60] R.D. Armstrong, M. Fleischmann, H.R. Thirsk, J. Electroanal. Chem. 11 (1966) 208.
[61] M.Y. Abyaneh, M. Fleischmann, J. Electroanal. Chem., 119 (1981) 187, 197.